

TIME-INTEGRATED GAMMA-RAY BURST SYNCHROTRON SPECTRA FROM BLAST WAVE/CLOUD INTERACTIONS

JAMES CHIANG¹

E. O. Hulburt Center for Space Research, Code 7653, Naval Research Laboratory, Washington DC 20375-5352

Submitted to The Astrophysical Journal, October 13, 1998

ABSTRACT

We show that the spectral shape of the low energy tails found for the time-integrated spectra of gamma-ray bursts, even in the absence of strong synchrotron cooling, can be significantly softer than the $\nu F_\nu \propto \nu^{4/3}$ asymptote predicted by synchrotron shock models. As we have noted in a previous work, blast wave deceleration via interaction with ambient material causes the characteristic electron injection energy to decrease in proportion to the bulk Lorentz factor of the blast wave, and under certain conditions, this effect will at least partially account for the observed increase in pulse widths with decreasing energy. This spectral softening can also be reflected in the time-integrated pulse spectrum. Using a simple model for the blast wave interaction with a dense cloud of material, we show that just below the νF_ν spectral peak the integrated spectrum behaves as $\nu F_\nu \sim \nu^{1/2}$ and rolls over to a $\nu^{4/3}$ dependence at lower energies, thus a spectral shape arises which is similar to that predicted for the spectrum of a strongly synchrotron-cooled electron population. We discuss the implications of this work in the context of models of burst light curve variability which are based on blast wave/cloud interactions.

Subject headings: gamma rays: bursts — radiation mechanisms: nonthermal

1. INTRODUCTION

Models of blast wave shells interacting with ambient density inhomogeneities have been proposed as a possible source of the variability seen in GRB light curves (e.g., Sari & Piran 1995). However, external shock models of this type have come under criticism, either because of the enormous blast wave energies which are required, $\gtrsim 10^{53}$ ergs (Sari & Piran 1997), or because of difficulties in producing the observed temporal structure (Fenimore, Madras, & Nayakshin 1996; Fenimore et al. 1998). With the measurement of the redshift and afterglow flux for GRB 971214 (Kulkarni et al. 1998), it is now clear that isotropic blast wave energies of $\gtrsim 10^{53}$ ergs do occur in some bursts. This result has motivated a more recent treatment by Dermer & Mitman (1998) of blast wave/cloud interactions and the production of complex burst light curves. In that work, the overall burst light curve structure was modeled, but the detailed spectral and temporal shape of individual pulses was not. We consider some aspects of these latter issues in this paper.

Several authors have analyzed the spectra of the prompt high energy emission from gamma-ray bursts (GRBs). In particular, data from the Burst and Transient Source Experiment (BATSE) aboard the *Compton Observatory* have provided detailed spectral information which continues to constrain models of emission from these objects. Among others, Katz (1994) and Tavani (1996) have argued persuasively that the spectral shape of the prompt emission from most bursts is due to synchrotron radiation produced by electrons accelerated by a relativistic shock. Such electrons will have a well-defined characteristic energy, and Katz (1994) has pointed out that in the absence of energy losses the instantaneous low energy tail of the synchrotron spectrum from these electrons will have spectral dependence $\nu F_\nu \propto \nu^\delta$ where the index $\delta = 4/3$ (Rybicki & Lightman 1979). Radiative or adiabatic losses will cause the electron energies to evolve so that the instantaneous spectral index will satisfy $\delta \leq 4/3$. If synchrotron cooling is the dominant energy loss mechanism, then just below the characteristic synchrotron pho-

ton energy the spectrum will have $\delta = 1/2$ (Cohen et al. 1997; Sari, Piran, & Narayan 1998).

From the examination of BATSE data, two recent studies indeed find that the above constraint appears to be met by a large majority of bursts. Cohen et al. (1997) find that the low energy spectral indices of all 11 GRBs they examined satisfy $\delta \leq 4/3$ and that for several bursts the index approaches $4/3$ at the lowest energies. Schaefer et al. (1998) consider spectra from over 100 bursts from BATSE and Ginga data and find that 90% of them appear to satisfy this limit as well. Of the remaining 10%, for only one burst can no mitigating complication, such as background uncertainties or data gaps, be found. For much of the energy range below the νF_ν peak, most of the spectral indices found by both groups lie at intermediate values well within the range $1/2 < \delta < 4/3$. Schaefer et al. form a composite spectrum of 19 bright BATSE bursts and provide a quantitative estimate of the characteristic index. They find that the low energy index of the composite spectrum is $\delta \simeq 0.77$. Cohen et al. suggest that intermediate values of δ result from the heterogeneous nature of the emitting material, presumably with some regions being strongly cooled and others less so. However, in a more recent study of a somewhat larger BATSE burst sample, Preece et al. (1998) claim that as many as 25% of the bursts studied violate the $\delta < 4/3$ limit. This implies that synchrotron radiation cannot be the source of the gamma-ray emission for these bursts. However, Preece also has noted that violations of this limit can depend upon the specific spectral model chosen to fit the data (see discussion in Schaefer et al. 1998).

In this paper we will concern ourselves exclusively with synchrotron radiation and processes which can soften the apparent low energy spectrum. In a previous paper (Chiang 1998), we showed how the reduction of the characteristic electron injection energy due to the deceleration of the blast wave results in a spectral softening such that burst pulses are broader at lower energies. Fenimore et al. (1995) have noted this phenomenon in BATSE burst data, and several authors have attributed it to syn-

¹Present Address: JILA, Campus Box 440, University of Colorado, Boulder CO 90309-0440

chrotron cooling (Kazanas, Titarchuk, & Hua 1998; Dermer 1998). In the present work, we show that the time-integrated spectrum of a relativistic blast wave shell interacting with a dense cloud of material naturally produces a low energy spectral index $\delta \simeq 1/2$ which rolls over to $4/3$ at lower energies. Again, this effect is due to blast wave deceleration and the corresponding reduction of the characteristic electron injection energy even in the absence of synchrotron cooling.

In the remainder of this paper, we present in §2 our model for the deceleration of the blast wave as it interacts with a dense cloud; in §3, we describe the evolution of the electron distribution function in the non-radiative limit and compute instantaneous and time-integrated spectra as well as pulse profiles at various energies; and finally, in §4, we discuss this work's implications for and applicability to actual burst models.

2. BLAST WAVE/CLOUD INTERACTIONS IN THE NON-RADIATIVE LIMIT

Although blast waves are generally treated as spherical, for the interaction of a blast wave shell with a cloud at large radius, R , we consider the portion of the shell which intercepts a sufficiently small cloud to be planar. This implies $l \ll R$, where l is the linear size of the cloud perpendicular to the trajectory of the blast wave. For the purposes of this paper, we assume that the blast wave shell has traveled through a vacuum from $R = 0$ until it encounters the cloud. It is therefore initially thin, cold and dense, the internal energy of the material from the initial fireball event having been converted to the bulk motion of the expanding material. The initial mass of the shell fragment intercepting the cloud is $M_0 = E_0 \mathcal{A} / 4\pi R^2 c^2 \Gamma_0$ where E_0 is the fireball energy, Γ_0 is the initial bulk Lorentz factor of the shell and $\mathcal{A} \sim l^2$ is the cross-sectional area of the cloud which we take to be constant. The evolution of the bulk Lorentz factor as a function of the penetration distance r into the cloud is given by energy and momentum conservation (cf. Chiang & Dermer 1998):

$$\Gamma(r) = \frac{\Gamma_0 M_0 + m(r)}{(M_0^2 + 2\Gamma_0 M_0 m(r) + m(r)^2)^{1/2}} \quad (1)$$

$$\simeq \frac{\Gamma_0 M_0}{(2\Gamma_0 M_0 m(r))^{1/2}}, \quad (2)$$

where $m(r) = \mathcal{A} n_{\text{ext}} m_p r$ is the cloud rest mass which has been swept-up as a function of r , and n_{ext} is the cloud number density. The approximate expression (eq. 2) is valid during the deceleration phase but while the shell Lorentz factor is still relativistic, i.e., for $\Gamma_0 > \Gamma \gg 1$. The deceleration phase occurs beyond a penetration depth $r_d = M_0 / \mathcal{A} n_{\text{ext}} m_p \Gamma_0$. We consider clouds which are sufficiently dense so that $r_d \ll r_0$ where r_0 is the size of the cloud along the trajectory of the blast wave shell.

Equation 1 corresponds to the non-radiative limit. This limit in turn places a constraint on the strength of the magnetic field generated during the shell/cloud interaction in which the synchrotron cooling timescale must exceed the dynamical timescale in the co-moving frame of the shell. We define the dynamical timescale as the time for the shell to cross the cloud. From eq. 2, we find $\tau_{\text{dyn}} \simeq (r_0/c)(m(r_0)/\Gamma_0 M_0)^{1/2}$, and using the familiar expressions for the synchrotron loss timescales we find $\tau_{\text{syn}} \simeq (m_e/m_p)^2 (c\sigma_T \zeta_c n_{\text{ext}} \xi_e \xi_B)^{-1} \tilde{\Gamma}^{-3}$. Here $\zeta_c \sim 4-7$ is the compression ratio of the shock in the instantaneously co-moving frame, $\tilde{\Gamma}$ is a characteristic bulk Lorentz factor over the traversal time of the cloud, and ξ_e and ξ_B are equipartition parameters for the electrons and magnetic field respec-

tively. These quantities are defined in the usual way: the characteristic electron injection Lorentz factor is $\gamma_e = \xi_e (m_p/m_e) \Gamma$, and the magnetic field energy density is given by $B^2/8\pi = \xi_B \zeta_c n_{\text{ext}} m_p c^2 \Gamma^2$ (Chiang & Dermer 1998). The resulting non-radiative constraint is then

$$\xi_e \xi_B \lesssim 18\pi \frac{m_p c^2}{\sigma_T} \left(\frac{m_e}{m_p}\right)^2 \frac{1}{\zeta_c} \frac{R^2}{E_0} \left(\frac{\Gamma_f}{\tilde{\Gamma}}\right)^3 \quad (3)$$

where Γ_f is the bulk Lorentz factor at $r = r_0$. Assuming $\Gamma_0 = 200$, we take a reasonable value to be $\Gamma_f = 20$ so that most of the bulk kinetic energy of the shell is converted to internal energy, but it nonetheless remains relativistic, and our approximations (e.g., eq. 2) still apply. Note that this expression is independent of the cloud density and size. For $E_0 = 10^{54}$ ergs, $R = 10^{16}$ cm, we have $\xi_e \xi_B \lesssim 10^{-6} (\Gamma_f/\tilde{\Gamma})^3$. This limit is similar to that for non-radiative evolution found by Chiang & Dermer (1998) for a spherical blast wave which interacts with a uniform external medium. More detailed calculations show that this limit is actually conservative. For $\tilde{\Gamma} = \sqrt{\Gamma_0 \Gamma_f} = \sqrt{10} \Gamma_f$, we can set $\xi_e = 10^{-1}$ and $\xi_B = 10^{-6}$ and will do so unless otherwise noted.

An appropriate cloud size can be inferred from pulse widths seen in actual burst data. Norris et al. (1996) examined the distribution of individual pulse widths for a large number of burst light curves. They found that widths range from 10^{-2} to 10 s. In the hope of applying the signal from the interaction we describe to individual pulses seen in actual burst data, we choose $\Delta t_{\text{pulse}} = 0.1$ s as an exemplary value. We will equate this to the traversal time for the blast wave to cross the cloud as inferred by a distant observer lying along the shell fragment trajectory. As we will see below, this will give an upper limit to the actual pulse width. We find $\Delta t_{\text{pulse}} \simeq r_0/4c\Gamma_f$. This yields $r_0 \lesssim 10^{13}$ cm. Solving for the accumulated cloud rest mass as a function of Γ , we obtain $m \simeq M_0 \Gamma_0 / 2\Gamma^2$ and find a cloud density $n_{\text{ext}} \gtrsim 10^7 \text{ cm}^{-3}$. We note that for an initial bulk Lorentz factor of $\Gamma_0 = 200$ and if we assume $l \sim r_0$ we have $l/R < 1/\Gamma_0$, so that we can largely ignore curvature effects in computing the pulse profiles (Fenimore et al. 1998).

3. RESULTS

3.1. Instantaneous and Time-Integrated Spectra

We now compute the electron distribution function in the co-moving frame of the shell. Since we are only concerned with the low energy tail of the synchrotron spectrum, we model the electron injection function at any given depth r to be a δ -function in energy: $dN/drd\gamma = \mathcal{A} n_{\text{ext}} \delta(\gamma - \gamma_e(r))$ where $\gamma_e(r) = \xi_e (m_p/m_e) \Gamma(r)$. Evaluating the δ -function and integrating over r , we find

$$\frac{dN}{d\gamma} \simeq \frac{M_0 \Gamma_0}{m_p} \frac{1}{\xi_e} \frac{m_e}{m_p} \Gamma^{-3} \quad (4)$$

$$\simeq \frac{M_0 \Gamma_0}{m_p} \left(\frac{1}{\xi_e} \frac{m_e}{m_p}\right)^2 \gamma^{-3}. \quad (5)$$

The instantaneous synchrotron spectrum from such an electron distribution will be flat with $\nu L_\nu \propto \nu^0$. As seen by an observer along the shell trajectory, this flat portion of the spectrum will obtain for energies $\varepsilon \equiv h\nu/m_e c^2$ bounded by

$$\varepsilon_{\text{max}} = 2 \left(\xi_e \frac{m_p}{m_e}\right)^2 \left(\frac{B_\infty}{B_{\text{crit}}}\right) \Gamma_0^2 \Gamma^2 \quad (6)$$

$$\varepsilon_{\min} = 2 \left(\xi_e \frac{m_p}{m_e} \right)^2 \left(\frac{B_\infty}{B_{\text{crit}}} \right) \Gamma^4, \quad (7)$$

where $B_\infty \equiv (8\pi\zeta_c n_{\text{ext}} m_p c^2 \xi_B)^{1/2}$ and $B_{\text{crit}} = m_e^2 c^3 / e\hbar = 4.4 \times 10^{13} \text{ G}$, and we have estimated the Doppler factor for the shell to be $\mathcal{D} \simeq 2\Gamma$, appropriate for an observing angle of zero. For $\varepsilon < \varepsilon_{\min}$ the spectrum will behave as $\nu L_\nu \propto \varepsilon^{4/3}$ while above ε_{\max} the spectrum will be sharply cut-off. The normalization of this spectrum can be estimated using the δ -function approximation for synchrotron radiation (Dermer, Sturmer, & Schlickeiser 1997):

$$\nu L_\nu \simeq \frac{2c\sigma_T B^2}{3} \left(\frac{B_{\text{crit}}}{B} \right)^{3/2} \left(\frac{\varepsilon}{\mathcal{D}} \right)^{3/2} \frac{dN}{d\gamma} \mathcal{D}^4 \quad (8)$$

$$\simeq \frac{32}{3} c^3 \sigma_T \left(\frac{m_p}{m_e} \right)^2 \zeta_c n_{\text{ext}} \xi_B \xi_e^2 M_0 \Gamma_0 \Gamma^6. \quad (9)$$

Here we note that for a νL_ν spectrum which is isotropic in the co-moving frame the amplification due to Doppler boosting is \mathcal{D}^4 .

Defining the observer time t_{obs} to begin at $r = r_d$, we use eq. 2 and find the time dependence of the bulk Lorentz factor to be $\Gamma \simeq (M_0 \Gamma_0 / 8\pi m_p n_{\text{ext}} A t_{\text{obs}})^{1/4}$. Hence, we have $\nu L_\nu \propto t_{\text{obs}}^{-3/2}$, $\varepsilon_{\max} \propto t_{\text{obs}}^{-1/2}$ and $\varepsilon_{\min} \propto t_{\text{obs}}^{-1}$. Therefore, for a given energy, the flat portion of the instantaneous νL_ν spectrum enters into a narrow observed band pass at energy ε at a time $t_{\min} \propto \varepsilon^{-1}$ and exits at a later time $t_{\max} \propto \varepsilon^{-2}$. The observed energy dependence of the time-integrated spectrum will then be given by

$$\left. \frac{dE}{dA} \right|_\varepsilon \propto \int_{t_{\min}(\varepsilon)}^{t_{\max}(\varepsilon)} t_{\text{obs}}^{-3/2} dt_{\text{obs}} = 2(t_{\min}^{-1/2} - t_{\max}^{-1/2}) \quad (10)$$

$$\sim \varepsilon^{1/2}. \quad (11)$$

The lower limit provides the dominant term and thus gives the spectral index $\delta = 1/2$. This energy dependence will extend from a maximum energy

$$\varepsilon_{\text{peak}} \simeq 2 \left(\xi_e \frac{m_p}{m_e} \right)^2 \left(\frac{B_\infty}{B_{\text{crit}}} \right) \Gamma_0^4 \quad (12)$$

to a break energy

$$\varepsilon_{\text{break}} \simeq 2 \left(\xi_e \frac{m_p}{m_e} \right)^2 \left(\frac{B_\infty}{B_{\text{crit}}} \right) \left(\frac{E_0}{8\pi m_p c^2 r_0 n_{\text{ext}} R^2} \right)^2. \quad (13)$$

This is the characteristic photon energy from the electrons injected at r_0 . At this break energy, we use eq. 9 and estimate the spectral fluence explicitly:

$$\left. \frac{dE}{dA} \right|_{\varepsilon=\varepsilon_{\text{break}}} \simeq \frac{1}{3\pi d_l^2} \frac{\sigma_T}{m_e^2 c^4} \zeta_c \mathcal{A} \xi_B \xi_e^2 \left(\frac{E_0}{4\pi R^2} \right)^3, \quad (14)$$

where d_l is the luminosity distance to the source. We have neglected factors of $(1+z)$ for the sake of brevity. Below the break energy, the spectrum will consist of the low energy synchrotron tail and behave as $\sim \varepsilon^{4/3}$. We also estimate the spectral fluence at the peak:

$$\left. \frac{dE}{dA} \right|_{\varepsilon=\varepsilon_{\text{peak}}} \simeq \frac{2}{3\pi d_l^2} \frac{m_p \sigma_T}{m_e^2 c^2} \zeta_c \mathcal{A} \xi_B \xi_e^2 \left(\frac{E_0}{4\pi R^2} \right)^2 \Gamma_0^2. \quad (15)$$

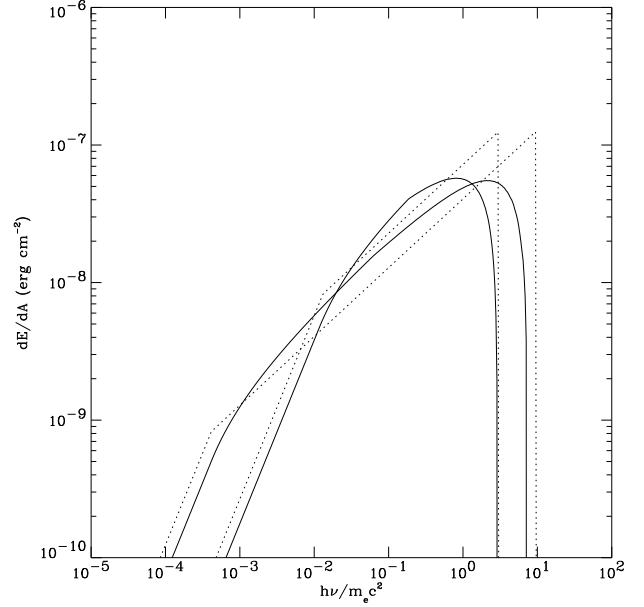


FIG. 1.— Time-integrated spectra for a blast-wave shell interacting with a small dense cloud. The solid curves are the numerical integrations and the dotted curves are the analytic estimates. Model parameters are $\Gamma_0 = 200$, $E_0 = 10^{54}$ ergs, $R = 10^{16}$ cm, $r_0 = l = 10^{13}$ cm, $\xi_e = 10^{-1}$, $\xi_B = 10^{-6}$, $d_l = 1.6 \times 10^{28}$ cm. The cloud density for the spectrum with the higher break energy is $n_{\text{ext}} = 10^7 \text{ cm}^{-3}$, while for the spectrum with the lower break energy $n_{\text{ext}} = 10^8 \text{ cm}^{-3}$ (see eq. 13).

In Figure 1 we plot the time-integrated spectra for a blast wave interacting with clouds of two different densities, $n_{\text{ext}} = 10^7$ and 10^8 cm^{-3} , keeping the other model parameters the same in both cases. The solid curves are spectra for which we have used the full expressions for the bulk Lorentz factor (eq. 1), the electron distribution function and the energy bounds for the flat part of the νL_ν spectrum. The only numerical approximations we used are the δ -function expression for the synchrotron emissivity and the assumption that below ε_{\min} the instantaneous spectrum has a $\varepsilon^{4/3}$ dependence. The dotted curves are our analytic estimates (eqs. 11–15) for the integrated spectra.

From these spectra and from eq. 13 we see that the location of the roll-over to the $\varepsilon^{4/3}$ spectral dependence is a sensitive function of several important burst parameters—namely, the isotropic fireball energy E_0 , the cloud size r_0 , the cloud density n_{ext} and the radial location of the cloud R . The quantity E_0 can be estimated by integrating up the total prompt burst and afterglow flux (e.g., Kulkarni et al. 1998 for GRB 971214), while R can be constrained via afterglow redshift and radio scintillation measurements as was done for GRB 970508 (Metzger et al. 1997; Frail et al. 1997). Note also that the initial bulk Lorentz factor Γ_0 is strongly constrained by equating $\varepsilon_{\text{peak}}$ with the energy of the spectral peak. This leaves the combination $n_{\text{ext}} r_0$ which is the column density through the cloud along the line-of-sight. The burst spectra depicted in Cohen et al. (1997), especially those of GRB 920406, GRB 910601 (rise) and GRB 930201, place an upper limit of ~ 1 decade on the range over which the $\nu^{1/2}$ dependence is seen. Equating this factor of 10 to the ratio $\varepsilon_{\text{peak}}/\varepsilon_{\text{break}}$, we obtain

$$n_{\text{ext}} r_0 \lesssim 10^{19} \left(\frac{E_0}{10^{54} \text{ erg}} \right) \left(\frac{R}{10^{16} \text{ cm}} \right)^{-2} \left(\frac{\Gamma_0}{200} \right)^{-2} \text{ cm}^{-2} \quad (16)$$

As we have shown above, individual pulse durations can then place additional limits on r_0 and n_{ext} , rendering all the physical parameters of the blast wave/cloud interaction reasonably well constrained.

In producing these fluence spectra, we have used a luminosity distance of $d_l = 1.6 \times 10^{28}$ cm, corresponding to a redshift of $z = 1$ with $H_0 = 67 \text{ km s}^{-1} \text{ Mpc}^{-1}$ and $q_0 = 0.5$. Thus even though we have considered very weak magnetic fields so that the electrons are not radiatively efficient, we see that for an individual pulse, the received fluence is in accord with total burst fluences which are typically seen. Approximately 20 of these sub-0.1 second pulses will be required to make up burst profiles with total fluences of order $\sim 10^{-6} \text{ erg cm}^{-2}$.

3.2. Pulse Profiles

At energies satisfying $\varepsilon_{\text{min}}(t_{\text{obs}}) < \varepsilon < \varepsilon_{\text{max}}(t_{\text{obs}})$, the temporal dependence of the light curve is $\sim t_{\text{obs}}^{-3/2}$. When $\varepsilon = \varepsilon_{\text{min}}(t_{\text{obs}})$, there will be a break in the light curve. This marks the transition from the $\varepsilon^{4/3}$ part of the instantaneous synchrotron spectrum to the ε^0 part. Inverting the expression for ε_{min} , we estimate the temporal break to occur at

$$t_{\text{obs, break}} \simeq 2 \left(\xi_e \frac{m_p}{m_e} \right)^2 \left(\frac{B_\infty}{B_{\text{crit}}} \right) \left(\frac{M_0 \Gamma_0}{8c A n_{\text{ext}} m_p} \right) \varepsilon^{-1}. \quad (17)$$

For observer times just prior to $t_{\text{obs, break}}$, the light curve will have a $t_{\text{obs}}^{-1/6}$ dependence. In Figure 2 we plot light curves obtained from the numerical calculations presented in Figure 1. The energies of these light curves are the lower bounds of the four standard BATSE LAD channels—25, 57, 115 and 320 keV (see Fenimore et al. 1995). The solid curves are the $n_{\text{ext}} = 10^7 \text{ cm}^{-2}$ calculation, while the dashed curves are the $n_{\text{ext}} = 10^8 \text{ cm}^{-2}$ case. Each light curve has been normalized to have maximum intensity of unity. The onset of the $t_{\text{obs}}^{-3/2}$ decline is delayed at lower energies according to $t_{\text{obs, break}} \propto \varepsilon^{-1}$. This energy dependence disagrees with the $\Delta t \propto \varepsilon^{-0.45}$ result found by Fenimore et al. (1995). However, at early times, when the observed flux at all energies of interest is due to the $\varepsilon^{4/3}$ portion of the spectra, the normalized light curves all decline together. So, in some average sense, the pulse widths in this model may be able to accommodate the energy dependence found by Fenimore et al..

4. IMPLICATIONS FOR BURST DATA AND MODELS

This model of GRB pulses produces a time-integrated spectral shape which is very similar to that expected for the spectrum of a strongly synchrotron-cooled electron distribution, even though synchrotron losses themselves are negligible. Therefore, spectral considerations alone may not be able to determine the importance of strong synchrotron cooling in prompt burst light curve variability. In particular, this model offers an alternative to the suggestion by Cohen et al. (1997) that the rapid variability seen in the light curve of GRB 930201 is due to short radiative timescales and that the $\delta \simeq 1/2$ spectral index in the time-integrated spectrum is corroborating evidence of this. The present picture is that the sharp spikes such as those in the GRB 930201 light curve are due to non-radiative blast-wave interactions with dense clouds. The short timescale variability and the spectral shape arise because of the quick deceleration of the blast wave. The former is largely controlled by the associated reduction in the amplification due to Doppler boosting

while the latter mostly results from the decreasing characteristic electron injection energy. As can be seen from Figures 1 & 2, larger cloud densities result in shorter pulse timescales and also in softer time-integrated spectra which is exactly the same correlation attributed to more efficient synchrotron cooling.

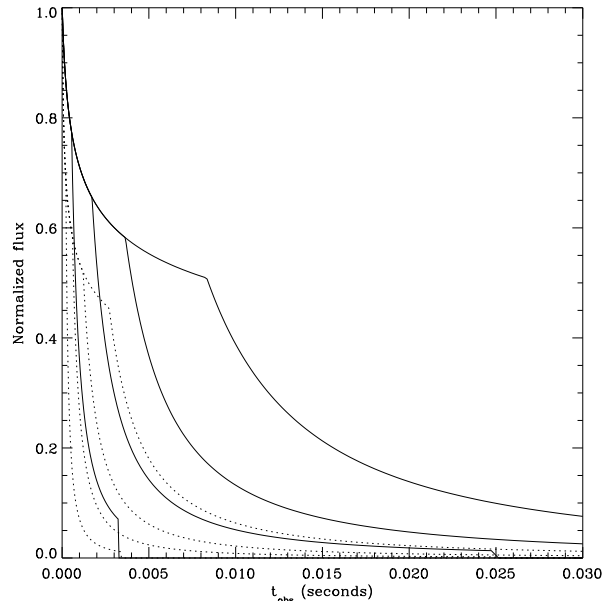


FIG. 2.— Blast wave/cloud burst pulse profiles at energies 25, 57, 115 and 320 keV which are the lower bounds of the four standard BATSE LAD channels. The narrower light curves correspond to the higher energies. The solid curves are produced using $n_{\text{ext}} = 10^7 \text{ cm}^{-2}$ and the dotted curves are for $n_{\text{ext}} = 10^8 \text{ cm}^{-2}$. All the other parameters are as given in Figure 1.

If synchrotron cooling were somewhat efficient, then we expect that the pulses would actually be broader in time. This would occur if the liberation of accumulated internal energy at later times acts to counter the reduction in received flux due to the broadening Doppler cone. This argument runs counter to the suggestion by Cohen et al. (1997) that shorter pulse durations should always be the result of shorter radiative timescales. However, if the blast wave interaction were *perfectly* radiatively efficient, then it does seem reasonable that the pulse durations would be shorter than in the non-radiative case we have examined here, not merely because of the shorter radiative timescales, but also because the bulk Lorentz factor would decline more rapidly. We suggest that it is in the intermediate case, where the dynamical timescale is a significant fraction of the synchrotron loss timescale, that the pulse durations will be longest.

Certain assumptions of this model force the time-integrated spectral index to be $\delta = 1/2$. In a spherical, rather than planar geometry, the time dependence of the bulk Lorentz factor during the deceleration phase will be $\Gamma \sim t_{\text{obs}}^{-g/(2g+1)}$ where g is the power-law index of the bulk Lorentz factor radial dependence, $\Gamma \propto R^{-g}$, where $3/2 < g < 3$ (Chiang & Dermer 1998; Dermer, Chiang, & Böttcher 1998). For non-radiative evolution, $g = 3/2$. Neglecting adiabatic losses, this implies a time dependence $\nu L_\nu \propto t_{\text{obs}}^{-9/4}$ or a time-integrated low energy spectral index of $\delta = 5/4$ (cf. eqs. 9 & 11). Inclusion of adiabatic losses may soften the spectrum further, but we note that the estimate by Cohen et al. (1997) of the effect of these losses for an expanding blast wave geometry, but neglecting some of the

effects of deceleration considered here, gives exactly this same spectral dependence.

Another important assumption is that the cloud density is a constant, independent of the penetration depth r . A density which decreases with r will leave the spectrum harder, while an increasing density will likely make the spectrum even softer. Likewise, a range of cloud column densities will have the effect of producing an intermediate spectral index for the composite spectrum integrated over many clouds. Furthermore, we note that even a single cloud will have an apparent index differing from $\delta = 1/2$ if the cloud column density is sufficiently small so that the break energy is relatively large and only the gradual roll-over to $\delta = 4/3$ is seen. The $n_{\text{ext}} = 10^7 \text{ cm}^{-3}$ case shown in Figure 1 is an example of this effect.

This model has several features which might make it difficult to fit into the context of realistic burst source models. First of all, clouds with densities of $\sim 10^7 \text{ cm}^{-3}$ in an otherwise evacuated surrounding environment may not be physically realizable. In models of AGNs, the dense clouds which are posited to compose the broad line region require a confinement mechanism such as a strong external magnetic field or hot external ambient matter in order that they not dissipate on the relevant timescales. If confinement is necessary for dense clouds around burst progenitors, it is not clear that either of these mechanisms is viable in GRB environments. In any case, the origin of such clouds is a genuine difficulty which needs to be addressed.

There are additional concerns regarding the geometry of the cloud region. From eq. 15, we see that the magnitude of the fluence at the spectral peak behaves as $dE/dA \propto R^{-4}$ for clouds of the same density and size. Therefore, in order for the pulses to have roughly equal fluence throughout the burst light curve, the clouds must either be confined to a narrow range in radius and essentially form a thin shell of clouds, or the cloud density and size distributions must compensate for the strong decline in fluence at larger radii. If the clouds are confined to a thin shell,

then for the parameters we have considered, only ~ 25 clouds would be required to cover the shell entirely within the initial Doppler beaming cone of the blast wave. Constraints such as this may place severe limits on the amount of variability which can be obtained in this model.

The microphysics of the relativistic shock also needs to be more carefully considered in all synchrotron shock models. We have assumed that the magnetic field energy density will always be a constant fraction of the energy density of the shocked material. There is no particular reason that this will be the case. Lastly, we have allowed the particle distributions to accumulate without regard to their effect on the state of the shocked fluid. If it is not radiated, some of this particle energy will result in the expansion of the shock region and there will then be adiabatic losses to consider.

Despite the numerous simplifications of this model of blast wave/cloud interactions, the central point is still quite valid: if synchrotron radiation from relativistic shocks is responsible for the prompt emission of GRBs, then the bulk deceleration of the shocked material can have a profound effect on the observed time-integrated spectra. Therefore any conclusions regarding the radiative efficiency of these shocks based upon spectral shapes must also consider these effects. More optimistically, if this model is relevant to burst temporal variability, then calculations such as this can provide a starting point for using GRB light curves as a probe of the circumburst environment and may then provide some insight into the actual progenitors of these events.

The author acknowledges helpful discussions with C. D. Dermer and E. E. Fenimore. I also thank M. A. Nowak for useful comments which have improved the text. Part of this work was performed while the author held a National Research Council-NRL Research Associateship.

REFERENCES

- Chiang, J. 1998, ApJ, 508, in press (astro-ph/980530)
 Chiang, J., & Dermer, C. D. 1998, ApJ, in press (astro-ph/9803339)
 Cohen, E., et al. 1997, ApJ, 488, 330
 Dermer, C. D., Sturmer, S. J., & Schlickeiser, R. 1997, ApJS, 109, 103
 Dermer, C. D. 1998, ApJ, 501, L157
 Dermer, C. D., Chiang, J., & Böttcher, M., 1998, ApJ, in press (astro-ph/9804174)
 Dermer, C. D., & Mitman, K. E. 1998, ApJL, submitted (astro-ph/9809411)
 Fenimore, E. E., et al. 1995, ApJ, 448, L101
 Fenimore, E. E., Madras, C. D., & Nayakshin, S. 1996, ApJ, 473, 998
 Fenimore, E. E., et al. 1998, ApJ, submitted (astro-ph/9802200)
 Frail, D., et al. 1997, Nature, 389, 261
 Katz, J. I. 1994, ApJ, 432, L107
 Kazanas, D., Titarchuk, L. G., & Hua, X.-M. 1998, ApJ, 493, 708
 Kulkarni, S. R., et al. 1998, Nature, 393, 35
 Metzger, M. R., et al. 1997, Nature, 387, 878
 Norris, J., et al. 1996, ApJ, 459, 393
 Preece, R. D., et al. 1998, ApJL, in press (astro-ph/9808184)
 Rybicki, G. B., & Lightman, A. P. 1979, Radiative Processes in Astrophysics (New York: Wiley)
 Sari, R., & Piran, T. 1995, ApJ, 455, L143
 Sari, R., & Piran, T. 1997, ApJ, 485, 270
 Sari, R., Piran, T., & Narayan, R. 1998, 497, L17
 Schaefer, B. E., et al. 1998, ApJ, 492, 696
 Tavani, M. 1996, ApJ, 466, 768